DETERMINATION OF THE PRESSURE DISTRIBUTION AND FLUCTUATIONS OF THE TRANSONIC FLOW IN A HIGHLY LOADED COMPRESSOR CASCADE

K. Hummel, C. Tiedemann, D. Peitsch, Chair for Aeroengines,
Department of Aeronautics and Astronautics,
Technische Universität Berlin, Marchstr. 12-14, 10587 Berlin, Germany

Abstract

In-depth analysis of secondary flow phenomena is essential for active flow control investigations for highly efficient aero engines. Therefore a linear stator cascade test facility for high speed flow conditions was established at the Institute of Aeronautics and Astronautics of the Technische Universität Berlin.
Center piece of the research is a linear cascade consisting of seven controlled diffusion airfoils featuring high loading and increased deflection. The design point is set to a Mach number of M = 0.75 and a Reynolds number of Re = $1.1 \cdot 10^6$ based on the axial chord. The center blade is equipped with high frequency, flush mounted pressure transducers that can be traversed perpendicular to the flow. This setup allows high spatial and temporal resolution of the blade pressure distribution and its fluctuations hence giving detailed information about three-dimensional secondary flow phenomena over the whole blade height. Furthermore an analysis of the base flow by oil flow pattern supports the understanding of the flow structures detected with the sensor equipped blade.
The main and secondary flow structures are investigated on the suction and pressure side under variation of incidence angle and inflow Mach number. The pressure distribution and its standard deviation give knowledge about the profile and secondary flow losses that are depending on size and intensity of the separation and the corner vortices. The analysis of the frequency spectrum of the static profile pressure shows flow structures like separation and shocks and their characteristic frequencies.

NOMENCLATURE

c	[mm]	Chord length
c_p	$[-]$	Pressure coefficient
D_H	$[-]$	DeHaller number
f	$[s^{-1}]$	Frequency
h	$[mm]$	Blade height
i	[°]	Incidence angle
M	$[-]$	Mach number
p	$[mbar]$	Pressure
Re	$[-]$	Reynolds number
t	[mm]	Pitch
β	[°]	Flow angle
γ	[°]	Stagger angle

Subscripts

amb	Ambient
0	Stagnation
1	Inlet plane
2	Outlet plane
Δ	Difference
s	Static
x	Local
∞	Inflow condition
max, min	Maximum, minimum
PS, SS	Pressure/ suction side

Abbreviations

CDA	Controlled Diffusion Airfoil
PSD	Power spectral density
RMS	Root mean square

1. INTRODUCTION

With an annual increase of worldwide air traffic by 4% to 5% it is essential to increase the efficiency of aircrafts. This affects the economic and environmental aspects – for pollution control [1]. A major contribution is the propulsion system.

To improve the efficiency of the engines, efforts are made in various directions, e.g. new materials, improvement of aerodynamics and increase of the thermodynamic parameters such as pressure and temperature ratios.

The pressure ratio of each compressor stage grows with increasing flow turning angles. This allows fewer stages and lighter engines with the same overall pressure ratio but leads to higher load on the blades.

For optimization of the flow at the blades, full knowledge of the whole flow field is essential. The structures are highly three dimensional and an examination with good spatial and temporal resolution is necessary. The spatial resolution gives the size of the secondary flow areas. The temporal resolution enables the characterization of the intensity of the fluctuations that also is a measure for the losses through secondary flows, e.g. corner vortices.

This work is focused on the determination of the pressure distribution and fluctuations on highly loaded compressor blades in transonic flow. Highly loaded blades have a high turning angle and thus high pressure increase. The

pressure distribution and the fluctuations of the flow are characterized through the profile parameters, deflection, pressure increase and deceleration as well as the secondary flow phenomena locations and intensity. The objective is to analyze the steady state data for aerodynamic characteristics and a spectral analysis of the fluctuation for the different types of primary and secondary flow structures.

The range of experiments spreads out to a variation of the incidence angle and inflow Mach number. These parameters influence the turning and separation characteristics that have to be investigated. Evaluation of profile Mach number and the pressure coefficient give detailed insight on primary and secondary flow characteristics and losses for different flow conditions. These secondary flow characteristics such as corner separation and the horseshoe vortex have been studied intensively over the past years in annular and linear test facilities [2], [3], [4]. However the mechanisms of secondary flows are not yet fully understood in detail, concerning the active flow control for the reduction of losses. Thus the flow conditions need to be investigated to find a frequency for the actuation and get an insight about the flow conditions with and without active flow control.

2. EXPERIMENTAL SETUP

At the Institute of Aeronautics and Astronautics of Technische Universität Berlin, a linear stator cascade with seven blades was designed. The setup of the cascade designed by Tiedemann et al. [5] allows the variation of the incidence angle up to $\pm 10°$ for the analyses of the separation characteristics at different inflow Mach numbers.
The flow in linear cascades is intensively investigated at the TU Berlin by Hecklau, Zander and Tiedemann [5], [6], [7], [8] in respect of active flow control and base flow analysis at different flow conditions. The linear cascade of Hecklau and Zander works under subsonic conditions, while the test facility used by Tiedemann operates under transonic conditions. For later experiments concerning active flow control, here the basic characteristics are determined.

2.1 Wind Tunnel

The linear cascade is installed as part of open wind tunnel with ambient outlet conditions. The test rig is supplied with a continuous airflow by three radial compressors with a pressure ratio of $\Pi = 2$ and a maximum mass flow rate of $1.5\ kg/s$ each. In different setups, the maximum mass flow rate reaches up to $4.5\ kg/s$ at a pressure ratio of $\Pi = 2$ or $3\ kg/s$ at $\Pi = 3.5$.

The wind tunnel consists of a diffusor, a settling chamber and a $44{:}1$ contraction nozzle with a rectangular outlet area of $181mm\ x\ 63mm$.

2.2 Cascade Test Section

A sketch of the stator cascade is shown in figure 1. Seven blades are installed to achieve pitchwise periodic flow conditions. At top and bottom of the two additional tailboards and boundary layer suction are implemented for the adjustment of uniformity of the inflow for all blades.
This is achieved by static pressure taps being installed half of the chordlength $(0.5\ c)$ upstream of the leading edge in the sidewall over the whole height of the cascade.
The measurements are carried out on the center blade of the cascade. For variation of the inflow angle, the cascade is mounted on a rotatable disk. Flexible sidewalls at the top and bottom are required for the adaption to the changing incidence angle.

For determination of the inflow Mach number M_∞, the total pressure p_0 is measured with a Pitot tube in the settling chamber of the wind tunnel. Here the losses due to deceleration of the fluid are small because of very low velocities compared to other measurement positions in the wind tunnel. The total temperature is also measured in the settling chamber with lowest forced convective heat transfer at measuring point to avoid errors in the measurements. The determination is necessary to calculate the density that plays an important role in transonic flows. Static pressure measurement p_∞ at the sidewall $0.5\ c$ upstream leading edge allows calculation of the inflow Mach number as shown in equation (1).

$$M_\infty = \sqrt{\left[\left(\frac{p_0}{p_\infty}\right)^{\frac{\kappa-1}{\kappa}} - 1\right]\frac{2}{\kappa-1}} \tag{1}$$

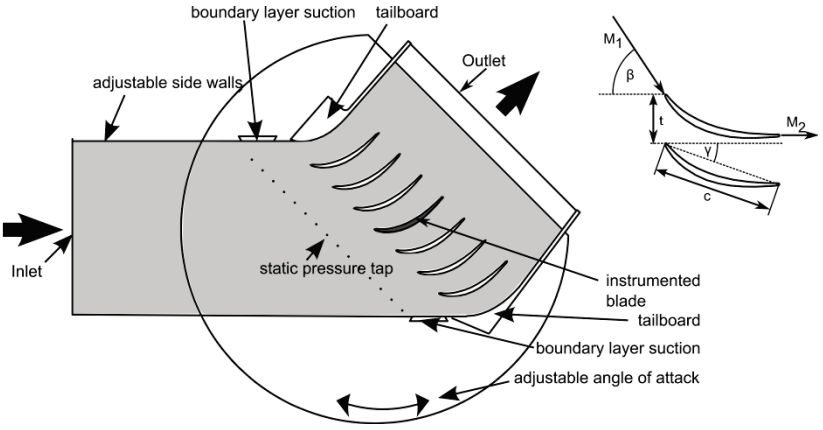

Figure 1. Cascade test section

Parameter	Value
Chord length	$c = 0.08m$
Aspect-ratio	$h/c = 0.8$
Pitch ratio	$t/c\ = 0.4$
Inflow angle	$\beta_1 = 45 - 65°$
Deflection	$\Delta\beta = 55°$
Stagger angle	$\gamma = 20°$
Reynolds Number	$Re_\infty = 1.1 \times 10^6$
Mach Number	$M_\infty = 0.75$

TAB 1. Blade geometry data

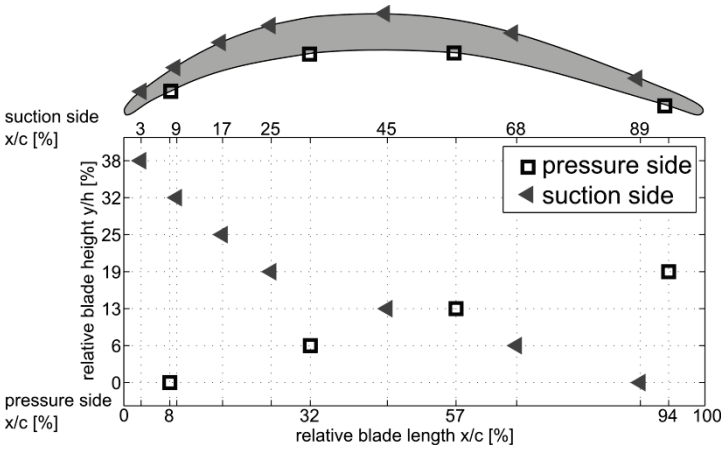

Figure 2. Pressure Measurement Positions

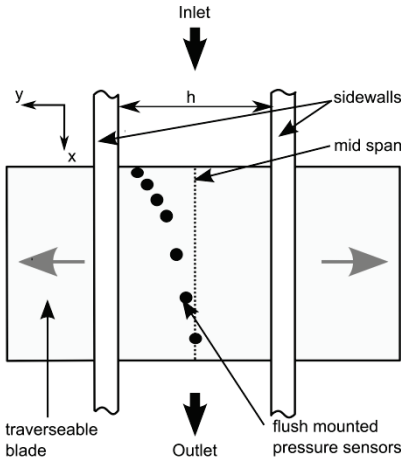

Figure 3. Sketch of the moveable blade

2.3 Blade and cascade design

The cascade and blades are specifically designed for secondary flow investigations. The compressor blade was designed as critically loaded transonic controlled diffusion airfoil (CDA) with MISES-calculation for an inflow Mach number of $M_\infty = 0.75$ and a Reynolds number of $Re_\infty = 1.1 \times 10^6$ based on the axial chord.

The blade has a very high deflection angle of $\Delta\beta = 55°$. That requires a small stagger ratio $(t/c = 0.4)$ to obtain the needed change in flow direction. The profile has an elliptical leading edge and a chord length of $c = 80\ mm$. For detailed investigations of secondary flow phenomena a small aspect ratio of $h/c = 0.8$ was chosen. So influence large regions of the blade flow are affected through these sidewall effects. Geometrical parameters are summarized in table 1.

2.4 Measurement techniques

To obtain the flow characteristics on the blade surface one blade is equipped with high frequency, flush mounted pressure transducers of the type Kulite LQ-47-1.7. The transducers have an Eigenfrequency of $240\ kHz$ and an achievable frequency resolution of $60\ kHz$ at a pressure range of $\pm 1700\ mbar$. The signals of the transducers are amplified and sequentially recorded with a sampling rate of $20\ kHz$. A hardware low pass filter with a cut-off frequency of $10\ kHz$ is used for anti-aliasing. For a sufficient time resolution, the measurement period of $120\ s$ is chosen. The datasets are divided into samples of 2^{15} points and transformed into frequency domain with an overlap of 50% to a resolution of $\Delta f = 0.61\ Hz$. An averaging of 100 ensembles suppresses the background noise [9].

The exact measurement positions of the pressure taps are shown in figure 2. On the suction side, 7 sensors are integrated into the blade's surface; on the pressure side 4 sensors are positioned. Figure 2 illustrates the positions of the sensors on the blade in terms of relative chord length x/c and relative blade height y/h. Relative suction side length of $x/c = 0\%$ corresponds to the leading edge of the profile. At $100\%\ x/c$ the trailing edge is located. The sensors are shifted in chordwise (x) and spanwise (y) direction. The offset in y-direction on pressure and suction side is $\Delta y/h = 6{,}3\%$ so an influence in main flow direction of the sensors to each other is reduced. The first sensor on the suction side in chordwise direction is positioned at $x/c = 3\%$ shown as rectangles at the top of the chart, while at the sensor positions on pressure side are displayed as squares. Due to the strong convex curvature on the suction side near the leading edge, the sensors are closely positioned in chordwise direction compared to the pressure side.

A sketch of this blade is shown in figure 3. It is traversable perpendicular to the flow allowing a high spatial resolution in spanwise direction through sequential measurements. The blade pressure distribution and fluctuations supply detailed information about three-dimensional secondary flow phenomena over the whole blade height. The blade is shifted by $\Delta y/h = 3{,}2\%$ for each measurement. The measurement blade is 2.9 times higher than test section width h. It is traversed through inserts in the side wall with a profile shaped extruded cut which are isolated from ambient conditions by a cover with a gasket placed outside the cascade. To achieve measurements of the whole blade height, 42 measurements are required.

3. RESULTS

The measurement of the static pressure at mid span of the blade provides pressure coefficient c_p and Mach number distribution M_x. The primary flow is investigated under nine different angles of attack and three inflow Mach numbers.

$$M_\infty = [0.6; 0.7; 0.75]$$

$$-5° \leq i \leq 3°$$

The analysis of mid span pressure distribution for all cases shows the profile characteristics like deceleration, deflection and pressure rise.
For in-depth analysis of secondary flow phenomena and flow characteristics at different Mach numbers and incidence angles, the blade is perpendicularly traversed though the cascade. A spectral analysis of the fluctuations over the whole blade height, give detailed information about the flow structures like separation and shocks and their characteristic frequencies.

The flow case with an inflow angle of $\beta = 55°$ $(i = 0°)$ at $M_\infty = 0.75$ is called base flow.

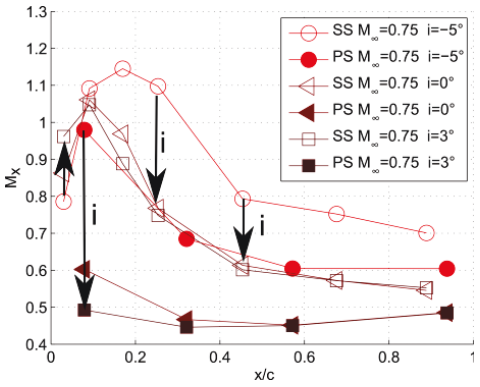

Figure 4. M_x distribution at midspan for different incidence angles

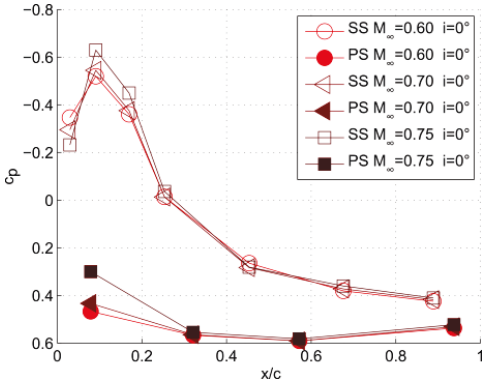

Figure 5. Pressure distribution at midspan for different inflow Mach numbers

3.1 Mid span

For basic analyses of the flow, the parameters at mid span are evaluated. The flow effects of the sidewall are assumed to be negligible. Nevertheless, with a small aspect ratio the streamlines in the middle are constricted by the side wall effect [4]. Due to the spanwise offset of the pressure transducers, seven measurements with traversing are necessary to get the mid span solution. As a result of the variation of the incidence angle, figure 4 shows the local Mach number distribution M_x, over relative blade chord x/c for pressure side and suction side.

The compressor cascade decreases the flow velocity from leading to trailing edge and therefore increases the static pressure. The flow speed on the suction side is supersonic at $M_\infty = 0.75$ for all incidence angles. Increasing the incidence angle at constant inlet Mach number leads to an increased suction peak. Also the Mach number M_{xSS} at $x/c = 3\%$ increases on the suction side near the leading edge due to flow acceleration at the elliptic curvature. Profile Mach number $M_{xPS}(8\%)$ on the pressure side drops significantly from the inflow speed.

For $i = 0°$ and $i = 3°$ the Mach number distribution in the rear part $(\mathrm{x/c} > 25\%)$ shows a good match on pressure and suction side. So the deceleration represented by the DeHaller number is the same at all inflow Mach numbers. It is in between $0.65 < D_H < 0.74$, build with $M_{xPS}(94\%)$ and $M_{xSS}(89\%)$ near the trailing edge.

For $i = -5°$ the profile Mach number distribution is shifted to higher M_x. As known from earlier oil flow investigations, a shock in the passage occurs and causes strong total pressure loss and a deceleration of the flow. The calculation of M_x (equation (2)) using the total pressure in the settling chamber neglects this total pressure loss due to the passage shock. This causes an overestimation of the profile Mach number M_x downstream of the shock position. It is shifted to higher Mach numbers on the suction an d pressure side of the blade.

$$M_x = \sqrt{\left[\left(\frac{p_0}{p_x}\right)^{\frac{\kappa-1}{\kappa}} - 1\right]\frac{2}{\kappa-1}} \quad (2)$$

The distribution of the pressure coefficient in figure 5 at mid span over the relative blade length shows similar characteristics for all inflow Mach numbers. M_x and the stage pressure are increasing with higher M_∞ in the front part of the blade.

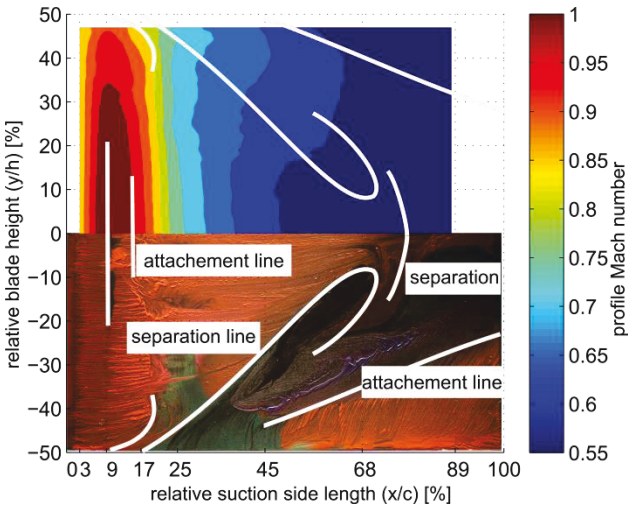

Figure 6. Oil flow visualization and profile Mach number for the base flow on the blade's suction surface

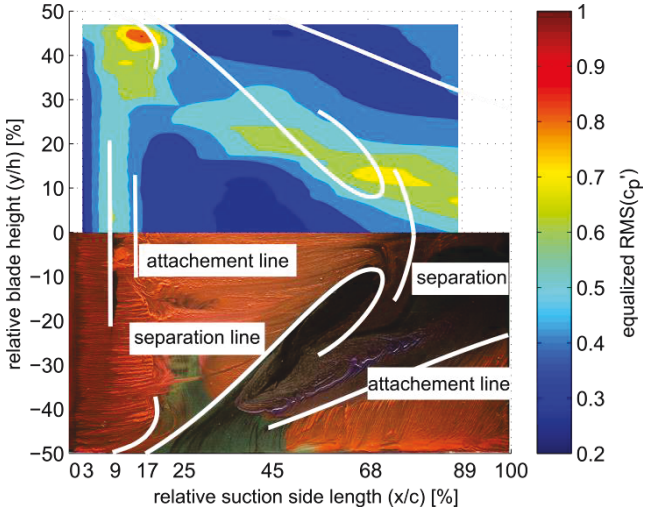

Figure 7. Oil flow visualization and RMS value of the pressure coefficient for the base flow on the blade's suction surface

3.2 Base flow analysis

The base flow analysis is performed for the suction side as a comparison of different measurement techniques, oil flow patterns and static pressure measurements, assuming a homogeneous inflow condition for all blades. The sidewall boundary layer at the blade leading edge has a displacement thickness of $6\%\ y/h$ of the blade height. The secondary flow characteristics that are of interest in this investigation are mainly influenced through these side wall boundary layers. Due to the small aspect ratio of $0.8\ h/c$ the flow is influenced in large regions through the sidewall effects.

3.2.1 Velocity flow field

Figure 6 compares the profile Mach number distribution at suction side for the base flow to the oil flow pattern. The point of view is normal to the chord. The side walls are located at the top and bottom of the diagram at $\pm 50\%\ y/h$. Relative blade height position $y/h = 0\%$ corresponds to mid span of the profile.

The oil flow pattern reveals dominant secondary flow phenomena on the suction side of the profile. In association with Zander and Hecklau [10], corner vortices cause a flow separation near the sidewall.

The laminar boundary layer separates shortly downstream the leading edge at mid span and reattaches turbulently at the attachment line. The Mach number distribution shows maximum velocity at mid span while the velocity decreases with further distance to the centerline. Furthermore the Mach number gradient downstream of the suction peak is larger than in the outer area of the blade, where the oil flow pattern reveals the corner vortices. The separation region of the corner vortices expands near the side walls and merges towards the centerline further downstream.

In comparison between oil flow pattern and velocity distributions, the spanwise velocity distribution, due to secondary flows, shows higher M_x at the position of the corner vortices than in mid span, where the flow decelerates properly. Downstream of $45\%\ x/c$, the corner vortex reattaches near the wall and the velocity in the reattached region is also lower than at the corner vortex position. At mid span, the turbulent boundary layer separates at $75\%\ \mathrm{x/c}$ resulting in a constant Mach number on the blade's surface. This separation is caused by the high blade turning angle.

3.2.2 Pressure fluctuations

For detailed analysis of the secondary flow structures the pressure fluctuations are evaluated by the root mean square (RMS) value of the pressure coefficient. Zander [10] proclaims that the RMS value of the pressure fluctuations is a suitable criterion to display the dominating flow structures. In experimental investigations of Belz [11], the amplitude of the $\mathrm{c_p}'$ on the suction side in the transonic case is twice as high as in subsonic flows and drops abruptly at the shock position.

Figure 7 shows the base flow, comparing the normalized RMS values of the pressure distribution with the oil flow patterns on the suction side. The RMS is calculated by $c_p' = c_p - \overline{c_p}$, where $\overline{c_p}$ is the time averaged pressure coefficient. $RMS(c_p')$ is normalized by its maximum value to allow comparison of different inflow conditions. The distribution of RMS-values does not match perfectly to the expected flow field phenomena of the oil flow patterns. The position of the corner vortex might be influenced through disturbances in the flow through the pressure taps even though they are not positioned in streamwise direction.

The oil flow visualization shows a laminar boundary layer near the leading edge at $9\%\ \mathrm{x/c}$. Here the RMS values are small due to the laminar flow characeristic. Near the sidewalls, the RMS is larger than in the middle of the passage. In mid span region the flow separates at $9\%\ \mathrm{x/c}$ and reattaches turbulently further downstream. The RMS value increases at the laminar separation bubble and reduces after reattachment. Near the leading edge, at the corner to the side wall, the horseshoe vortex develops and causes further fluctuations. The boundary layer at the side wall decelerates at the leading edge and rolls up to a vortex. An overlay of the horseshoe vortex with the passage vortex is building the corner vortex. Where the corner vortex spreads out, RMS values are higher than in the surrounding areas. This region is shifted towards mid span further downstream, according to the separation line of the corner vortex. According to Gmelin [12], at the chordwise position of the reattachment of the separation bubble, strong secondary flows caused by the end walls come into effect. Near the side wall, fluctuations due to the corner vortex calm down as the vortex reattaches. At mid span, where the separation occurs, the RMS values are high and strongly influenced by the corner vortex.

Comparing all measurements for different incidence angles and inflow Mach numbers, the RMS values of the pressure coefficient increases as the flow accelerates and decreases at deceleration.

As proven by Zander and Hecklau [7], the RMS value is a suitable criterion to display the dominating secondary flow characteristics. The position and intensity of the losses due to secondary flow can be estimated, regarding different incidence angle and velocities. These fluctuations shall be matched to characteristic frequencies.

3.2.3 Frequency characteristics

The analysis of the power spectral density (PSD) reveals characteristic frequencies of the secondary flow characteristics that can be used for an actuation of the flow. Purpose of determination was to find an effective frequency and position for active flow control of the separated regions to reduce the losses through the corner vortices on the transonic compressor blade. For span and chordwise direction, the frequencies were analyzed for several inflow Mach numbers and incidence angles.

As a result for the base flow conditions, the flow field has a steady character, so no dominant frequency was found in the passage that could be used as a forcing frequency. The PSD for the base flow shows no amplitudes that would give a clear indication of secondary flow characteristics. The corner vortex could not be related to a characteristic frequency. On the pressure side of the profile, only the horseshoe vortex is present. No characteristic frequencies could be detected here. The fluctuations of the vortices appear in the RMS value distribution and the oil flow pattern but not in the PSD.

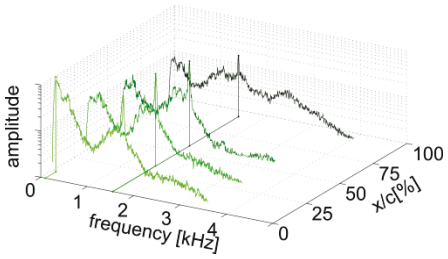

Figure 8. PSD of PS at mid span for $\boldsymbol{i = 3°}$

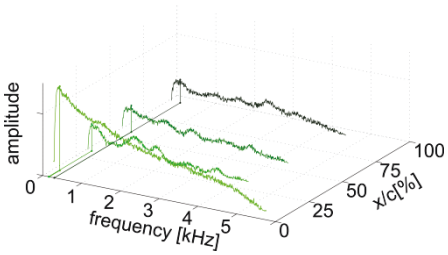

Figure 9. PSD of PS at mid span for $\boldsymbol{i = 0°}$

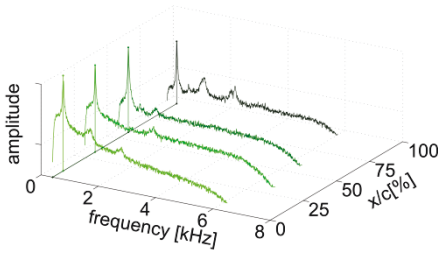

Figure 10. PSD of PS at mid span for $\boldsymbol{i = -5°}$

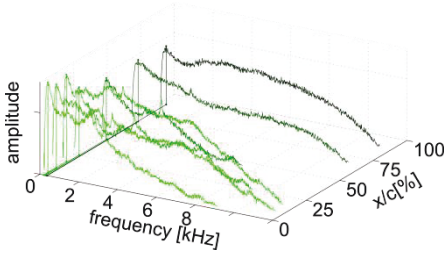

Figure 11. PSD of SS at mid span for $\boldsymbol{i = 3°}$

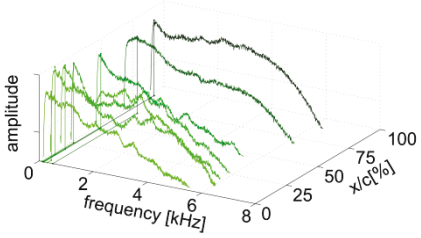

Figure 12. PSD of SS at mid span for $\boldsymbol{i = 0°}$

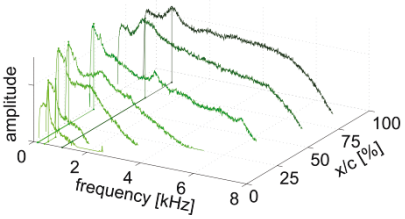

Figure 13. PSD of SS at mid span for $\boldsymbol{i = -5°}$

In contrast to the base flow, the separation at $i = 3°$ and the passage shock at $i = -5°$ reveal characteristic frequencies. These cases are discussed in detail in the following.

For the inflow Mach number of $M_\infty = 0.75$ an analysis of the PSD for different incidence angles in mid span is accomplished. The analysis compares the spectrum on the pressure and suction side in mid span to evaluate the dependencies of the primary flow from the incidence angle. In all figures 8 to 13 the PSD with amplitude and frequency are plotted over relative blade length x/c. In the figures at the top (figure 8 to 10) the PSD of the pressure side at the positions 8%, 32%, 57% and $94\%\, x/c$ are displayed. For suction side fluctuations, the figures 11 to 13 show the spectra also with decreasing incidence angles from left to right.

Concretely, the PSD of the pressure side for an incidence angle of $\mathrm{i} = 3°$ in figure 8 shows a characteristic frequency at $1.55\ \mathrm{kHz}$. This corresponds to a reduced frequency of $f^+ = 0.49$ calculated with equation (3).

$$f^+ = \frac{f \cdot c}{u_\infty} \tag{3}$$

As known from earlier investigations by oil flow pattern the flow is separated in this case. This reduced frequency of $f^+ = 0.49$ is allocated to the flow separation at high incidence angles ($i = 3°$). An analysis of smaller incidences shows a reduction of the amplitude for smaller incidence angles at the same reduced frequency of $f^+ = 0.49$. At smaller inflow Mach numbers ($\mathrm{M}_\infty = 0.70$) the characteristic frequency does not appear, because the flow is not highly loaded and does not separate. Also on the suction side at $\mathrm{i} = 3°$ (figure 11), the frequency of $f^+ = 0.49$ is detected from the leading edge downstream to $45\%\ \mathrm{x/c}$. The sensors at 68% and $89\%\ \mathrm{x/c}$ show broadband noise that could not be eliminated by filtering.

Increasing the incidence angle to $\mathrm{i} = 0°$ in figure 9 and figure 12, no characteristic peak appears in mid span in the PSD. Also investigations of the spectra in spanwise direction do not show specific frequency peaks. For the corner vortices on the suction side, no characteristic frequency is detected. Due to the fact, under base flow conditions no shock or separation appears, there is no characteristic frequency.

As mentioned earlier, a passage shock occurs within the cascade at an incidence angle of $i = -5°$. The diffusion on the suction side is not moderate and the deceleration of the flow is accompanied by a strong shock. On the pressure side (figure 10) a peak appears with a frequency of $410\ Hz$ (corresponding to a reduced frequency of $f^+ = 0.13$). This frequency clearly belongs to the shock. At smaller inflow Mach numbers of $M_\infty = 0.70$ with the same incidence angle, no shock is expected in the passage because the flow is subsonic. On the suction side in mid span, the amplitude of the shock frequency is small at $3\%\ \mathrm{x/c}$ and increases further downstream. At $17\%\ \mathrm{x/c}$ supersonic conditions are reached. The high amplitude at the frequency of $410\ Hz$ is higher on the suction side and spreads out up to $45\%\ x/c$. Further downstream the broadband noise interferes the spectrum. The passage shock is oscillating in the passage over the whole blade height with a frequency of $f^+ = 0.13$ and initiates a blade vibration. This peak is only detected under these specific inflow conditions. On the pressure side (figure 13) the frequencies of $1.57\ kHz$ and $2.46\ kHz$, corresponding to $f^+ = 0.49$ and $f^+ = 0.77$ are detected. Due to very low incidence angles the flow separates on the suction side. In two cases of separation, at $i = 3°$ and $i = -5°$, the characteristic frequency of $f^+ = 0.49$ is detected. The separation refers to this frequency.

CONCLUSIONS

Experimental investigations were performed on a highly loaded, transonic compressor cascade. The flow was investigated with miniature pressure transducers for time resolved measurements of the static pressures under steady state inflow conditions. A characterization of the profile properties was done under various inflow Mach numbers and incidence angles.

The analysis of mid span pressure distribution for all cases revealed the profile characteristics like deceleration, deflection and pressure rise.

For in-depth analysis of secondary flow phenomena and flow characteristics a spectral analysis of the fluctuations over the whole blade height give detailed information about the flow structures like separation and shocks and their characteristic frequencies.

The objective was to determine an actuation frequency for the active flow control of the secondary flow in order to achieve higher compressor efficiencies.

Under base flow conditions the flow field has a very steady character, so no dominant frequency could be found in the passage. The corner vortices did not match to a characteristic frequency. The corner vortex could not be related to a characteristic frequency. There was no actuation frequency found by this method for the reduction of the losses in the passage though corner vortices. So in later investigations, the actuation frequency and positions is changed to reveal the best actuation frequency for smallest losses.

But in flow conditions where flow separation and shocks in this cascade are known to occur, the search of a characteristic frequency finally was successful. Characteristic frequencies were determined for the separation of $f^+ = 0.49$ and a reduced frequency of $f^+ = 0.13$ for the shock.

Further research is required to derive actual flow control mechanisms from these findings. Yet this research shows the potential of the method of the determination of pressure distribution and fluctuations of the transonic flow in a highly loaded compressor cascade to attain higher efficient engine designs.

ACKNOWLEDGMENTS

This work was carried out at the TU Berlin within a Diploma Thesis under supervision of Christine Tiedemann and Dieter Peitsch, as a part of the framework of the Collaborative Research Centre 557 “Control of turbulent shear flows”, supported by the German Research Foundation (DFG).

REFERENCES

[1] H. L. Group, “Flightpath 2050 Europe ’ s Vision for Aviation,” *Report of the High Level Group on Aviation Research.*

[2] S. A. Gbadebo, N. A. Cumpsty, and T. P. Hynes, “Three-Dimensional Separations in Axial Compressors,” *Journal of Turbomachinery*, vol. 127, no. 2, pp. 331–339, 2005.

[3] G. Thaler, K. Kuhn, and H. Jaberg, “Sekundärströmung in Schaufel(ring)gittern mit Pfeilung und V-Stellung - eine Literaturstudie,” in in *Forschung im Ingenieurwesen*, vol. 65, Springer-Verlag, 2000, pp. 236–246.

[4] A. Hergt, R. Meyer, and K. Engel, “Effects of Vortex Generator Application on the Performance of a Compressor Cascade,” *ASME Journal of Turbomachinery*, vol. 135, no. 021026–1, pp. 1–13, 2013.

[5] C. Tiedemann, A. Heinrich, and D. Peitsch, “A New Linear High Speed Compressor Stator Cascade for Active Flow Control Investigations,” *6th AIAA Flow Control Conference*, vol. 3251, pp. 1–11, 2012.

[6] C. Tiedemann, D. Peitsch, S. Steinberg, and R. King, “Identifikation einer Regelgröße zur aktiven Strömungskontrolle an einer linearen Verdichterkaskade im kompressiblen Machzahlbereich,” *DLRK*, no. 281267, pp. 1–10, 2012.

[7] V. Zander, M. Hecklau, and W. Nitsche, “Active control of corner vortices on a highly loaded compressor cascade,” *8th European Turbomachinery Conference, Graz*, no. 157, pp. 1–10, 2009.

[8] C. Beselt, R. Van Rennings, F. Thiele, and D. Peitsch, “Experimental and numerical investigation of rotating instability phenomenon in an axial compressor stator,” *42th AIAA Fluid Dynamics Conference, New Orleans*, vol. 2980, pp. 1–10, 2012.

[9] J. Bendat and A. Piersol, *Engineering applications of correlation and spectral analysis*. Wiley-Interscience Publication, 1980, p. 315.

[10] V. Zander and M. Hecklau, “Experimentelle Methoden zur Charakterisierung der aktiven Strömungskontrolle in einer hoch belasteten Verdichterkaskade,” *Deutscher Luft- und Raumfahrtkongress*, vol. 081322, 2008.

[11] J. Belz, H. Hennings, and G. Kahl, “Experimental investigation of the forcing function and forced pitching blade oscillations of an annular compressor cascade in transonic flow,” *ASME Turbo Expo , Glasgow*, vol. 23590, pp. 1–9, 2010.

[12] C. Gmelin, V. Zander, A. Huppertz, M. Swoboda, M. Hecklau, F. Thiele, and W. Nitsche, “Active Flow Control Concepts on a Highly Loaded Subsonic Compressor Cascade: Resume of Experimental and Numerical Results,” *Journal of Turbomachinery*, vol. 134, no. 6, p. 9, 2012.